A Multipronged Unbiased Strategy Guides the Development of an Anti-EGFR/EPHA2–Bispecific Antibody for Combination Cancer Therapy

Amr El Zawily[1,2], Frederick S. Vizeacoumar[1], Renuka Dahiya[1], Sara L. Banerjee[3], Kalpana K. Bhanumathy[1], Hussain Elhasasna[1], Glinton Hanover[1,4], Jessica C. Sharpe[5], Malkon G. Sanchez[1,4], Paul Greidanus[1,4], R. Greg Stacey[6], Kyung-Mee Moon[6], Ilya Alexandrov[7], Juha P. Himanen[8], Dimitar B. Nikolov[9], Humphrey Fonge[10,11], Aaron P. White[4,12], Leonard J. Foster[6], Bingcheng Wang[13], Behzad M. Toosi[5], Nicolas Bisson[3], Tajib A. Mirzabekov[7], Franco J. Vizeacoumar[14], and Andrew Freywald[1]

ABSTRACT

Purpose: Accumulating analyses of pro-oncogenic molecular mechanisms triggered a rapid development of targeted cancer therapies. Although many of these treatments produce impressive initial responses, eventual resistance onset is practically unavoidable. One of the main approaches for preventing this refractory condition relies on the implementation of combination therapies. This includes dual-specificity reagents that affect both of their targets with a high level of selectivity. Unfortunately, selection of target combinations for these treatments is often confounded by limitations in our understanding of tumor biology. Here, we describe and validate a multipronged unbiased strategy for predicting optimal co-targets for bispecific therapeutics.

Experimental Design: Our strategy integrates *ex vivo* genome-wide loss-of-function screening, BioID interactome profiling, and gene expression analysis of patient data to identify the best fit co-targets. Final validation of selected target combinations is done in tumorsphere cultures and xenograft models.

Results: Integration of our experimental approaches unambiguously pointed toward EGFR and EPHA2 tyrosine kinase receptors as molecules of choice for co-targeting in multiple tumor types. Following this lead, we generated a human bispecific anti-EGFR/EPHA2 antibody that, as predicted, very effectively suppresses tumor growth compared with its prototype anti-EGFR therapeutic antibody, cetuximab.

Conclusions: Our work not only presents a new bispecific antibody with a high potential for being developed into clinically relevant biologics, but more importantly, successfully validates a novel unbiased strategy for selecting biologically optimal target combinations. This is of a significant translational relevance, as such multifaceted unbiased approaches are likely to augment the development of effective combination therapies for cancer treatment.

See related commentary by Kumar, p. 2570

Introduction

A critical limitation of both traditional and emerging single-agent targeting cancer therapies is their common tendency to leave behind resistant cancer cell populations. This often happens because of the innate heterogeneity of molecular mechanisms supporting tumor cells, which allows survival and eventually, selective evolution of treatment-refractory and more aggressive clones. Accumulation of these resistant cells practically unavoidably concludes in tumor relapse and patient lethality (1). Therefore, combination therapies with their individual components targeting distinct cancer-related molecular mechanisms in a precise coordination are urgently required to improve therapeutic effects. Currently, the systematic design of optimal combinatorial approaches is only beginning to be explored and is not yet commonly used (1–3). To assist in addressing this challenge, we describe here an unbiased

[1]Department of Pathology and Laboratory Medicine, College of Medicine, University of Saskatchewan, Royal University Hospital, Saskatoon, Saskatchewan, Canada. [2]Department of Biology, College of Liberal Arts and Sciences, University of Iowa, Iowa City, Iowa. [3]Department of Molecular Biology, Medical Biochemistry and Pathology, PROTEO and Centre de recherche du Centre Hospitalier Universitaire (CHU) de Quebec-Université Laval, Division Oncologie, Québec, Canada. [4]Department of Biochemistry, Microbiology and Immunology, University of Saskatchewan, Health Sciences, Saskatoon, Saskatchewan, Canada. [5]Department of Small Animal Clinical Sciences, Western College of Veterinary Medicine, University of Saskatchewan, Saskatoon, Canada. [6]Michael Smith Laboratories and Department of Biochemistry and Molecular Biology, University of British Columbia, Vancouver, British Columbia, Canada. [7]Biomirex Inc., Natick, Massachusetts. [8]Department of Biochemistry, University of Turku, Turku, Finland. [9]Structural Biology Program, Memorial Sloan-Kettering Cancer Center, New York, New York. [10]Department of Medical Imaging, College of Medicine, University of Saskatchewan, Saskatoon, Saskatchewan, Canada. [11]Department of Medical Imaging, Royal University Hospital, Saskatoon, Saskatchewan, Canada. [12]Vaccine and Infectious Disease Organization-International Vaccine Centre, University of Saskatchewan, Saskatoon, Saskatchewan, Canada. [13]Division of Cancer Biology, Department of Medicine, MetroHealth Medical Center, and Case Western Reserve University School of Medicine, Case Comprehensive Cancer Center, Cleveland, Ohio. [14]Cancer Research, Saskatchewan Cancer Agency and Division of Oncology, University of Saskatchewan, Saskatoon, Saskatchewan, Canada.

A. El Zawily and F.S. Vizeacoumar contributed equally as co-authors of this article.

Corresponding Authors: Andrew Freywald, University of Saskatchewan, Room 2841, Saskatoon, Saskatchewan, S7N 0W8, Canada. Phone: 306-966-5248; E-mail: andrew.freywald@usask.ca; Franco J. Vizeacoumar, franco.vizeacoumar@usask.ca; Tajib A. Mirzabekov, tmirzabekov@biomirex.com; Nicolas Bisson, Nick.Bisson@crchudequebec.ulaval.ca; and Behzad M. Toosi, Behzad.toosi@usask.ca

Clin Cancer Res 2023;29:2686–701

doi: 10.1158/1078-0432.CCR-22-2535

Translational Relevance

Intensive efforts are currently focused on identifying effective therapeutic target combinations to combat cancer treatment resistance caused by tumor heterogeneity. Here, we describe and validate a multipronged unbiased strategy for selecting optimal co-targets for bispecific therapeutic reagents. Following its predictions, we generated a novel bispecific anti-EGFR/EPHA2 antibody. As predicted, the antibody produced strong tumor-suppressing effects compared with the therapeutic anti-EGFR cetuximab, which we used as a prototype for the EGFR-targeting arm of our bispecific molecule. Although EGFR is overactivated in multiple cancers, antitumor effects of its inhibitors are limited by compensatory molecular mechanisms. Taken in this context, our work provides a new biologic expected to benefit treatment of multiple malignancies. Of even higher translational relevance, the robust tumor suppression caused by co-targeting molecules selected by our strategy highlights its applicability for developing combinatory treatment approaches. Application of this strategy should facilitate the identification of optimal target combinations for bispecific therapeutics.

multifaceted strategy for selecting effective target combinations for novel dual-specificity reagents for cancer treatment.

The proposed strategy is based on the application of genome-wide loss of function *ex vivo* screening (4) for genetic dependencies acquired by xenograft tumor cells in response to a single-target reagent of choice. This is complemented by the profiling of the target's interactome using BioID proximity proteomics (5). Bioinformatics analyses–based overlapping the screening and interactome datasets allow to predict most promising target combinations (**Fig. 1A**). The relevance of the predicted target combinations is further assessed by gene expression analyses of patient data from the Cancer Genome Atlas (TCGA) database to select candidate co-targets frequently co-expressed in tumors. Finally, the anticancer efficiency of suppressing the selected target combinations is examined in cell culture and xenograft models (**Fig. 1A**).

The EPHA2 receptor tyrosine kinase (RTK) often supports tumor aggressiveness, is considered a promising target for cancer therapy (6) and is prioritized by NIH as a cancer-related antigen (7). Multiple attempts have been made to interfere with EPHA2 activity in cancer cells and although some of these approaches hold promise (6), none of the attempts have yet produced a clinically relevant therapeutic reagent. Therefore, to test the applicability of our approach, we focused our efforts on the EPHA2 receptor.

To implement our strategy, we generated a novel synthetic anti-EPHA2 antibody, used it to treat xenograft tumors and generated *ex vivo* cell populations from the treated and matching control xenografts. Application of our multipronged unbiased approach in this model guided us with a high level of confidence toward choosing the EGF receptor (EGFR) for co-targeting with EPHA2. Following this lead and to assess the accuracy of the selection, we used a therapeutic anti-EGFR antibody, cetuximab, as a prototype to design a human bispecific anti-EGFR/EPHA2 antibody, which as predicted, produced strong antitumor effects in xenograft models.

Taken together, our work reported here outlined and successfully validated an efficacious unbiased strategy that can be used for identifying optimal candidate targets for designing novel, highly potent bispecific therapeutics.

Materials and Methods

Antibodies, recombinant proteins, cell culture, and xenograft models

Details are provided in Supplementary Materials and Methods. All animal work protocols were approved by the Animal Research Ethics Board at the University of Saskatchewan. All *in vivo* experiments were carried out in accordance with established guidelines and regulations.

Expression and purification of Fabs and IgG

EPHA2-specific Fab fragments selected from antibody libraries were re-cloned into the pET22a plasmid and expressed in the periplasm of BLgold. After growing bacteria to $OD_{600} = 0.5$, Fab expression was induced by addition of 1 mmol/L IPTG and incubation of culture at 28°C for 15 hours. Fabs were expressed with heavy chain C-terminal c-Myc and His6 tags (CH-AAA-c-Myc-GAALE-His6) for assisting purification and detection. Fab fragments were purified using Ni^{+}-resin (Profinity IMAC Resin, Ni-charged, Bio-Rad, 1560135).

IgGs were expressed in CHO-S culture grown in Dynamis medium (Thermo Fisher Scientific, A2661501) following transfection with the FectoPro reagent (Polyplus Transfection, 116–010). The antibodies were harvested on days 12–14 after transfection and purified using MabSelect resin (GE Healthcare, 17–5199–01). After binding in PBS, the antibodies were eluted with 100 mmol/L citrate buffer (pH 3.0) followed by immediate titration to pH = 5.5 using 1 mol/L Tris-HCl, pH = 8.0. The eluted protein was dialyzed against and stored in the formulation buffer composed of 20 mmol/L L-Histidine, 30 mmol/L Citric acid, 32 mmol/L Na_2HPO_4, pH = 6.0, 1% trehalose, 0,05% Tween-20.

Pooled shRNA screening, computational, and statistical analyses

Pooled shRNA screening was performed and analyzed as previously described (8). Briefly, αEPHA2-Cond and cIgG-Tr cells were transduced with lentiviral particles expressing *sh*RNA library with approximately 200-fold hairpin representation. Cells were collected every 3 days for genomic DNA extraction and maintained at 200-fold coverage. Genomic DNA was extracted from cell pellets using the QIAamp Blood Maxi Kit (Qiagen). Genomic DNA was amplified by large-scale PCR and hybridized to micro array chips. Signal intensity from microarray was normalized with cyclic loess normalization and hairpins with low signal at timepoint T0 were removed before we calculated the differential cumulative change (DCC) between αEPHA2-Cond and cIgG-Tr cells. As the screens were done with two timepoints (T0 and T14), a modified version of the function was used with the following formula:

$$DCC = \left(x_{t14,rep}^{\alpha EPHA2-Cond} - x_{t0,rep}^{\alpha EPHA2-Cond}\right) - \left(x_{t14,rep}^{cIgG-Tr} - x_{t0,rep}^{cIgG-Tr}\right),$$

where $x_{t14,rep}^{\alpha EPHA2-Cond}$ is the normalized signal intensity at T14 and $x_{t0,rep}^{\alpha EPHA2-Cond}$ is the normalized signal intensity at T0 in replicates $rep \in (1..2)$ for αEPHA2-Cond cells. Likewise, $x_{t14,rep}^{cIgG-Tr}$ and $x_{t0,rep}^{cIgG-Tr}$ are for cIgG-Tr cells. We used 2 best hairpins with the most negative value for that gene to calculate the gene level DCC. To identify hairpins and their corresponding genes that are significantly different between the αEPHA2-Cond and cIgG-Tr cells, we used the Student *t* test in combination with the permutation test *P* value by estimating the frequency of randomized, shuffled DCC with more negative values in comparison with the observed gene level DCC value. Microarray

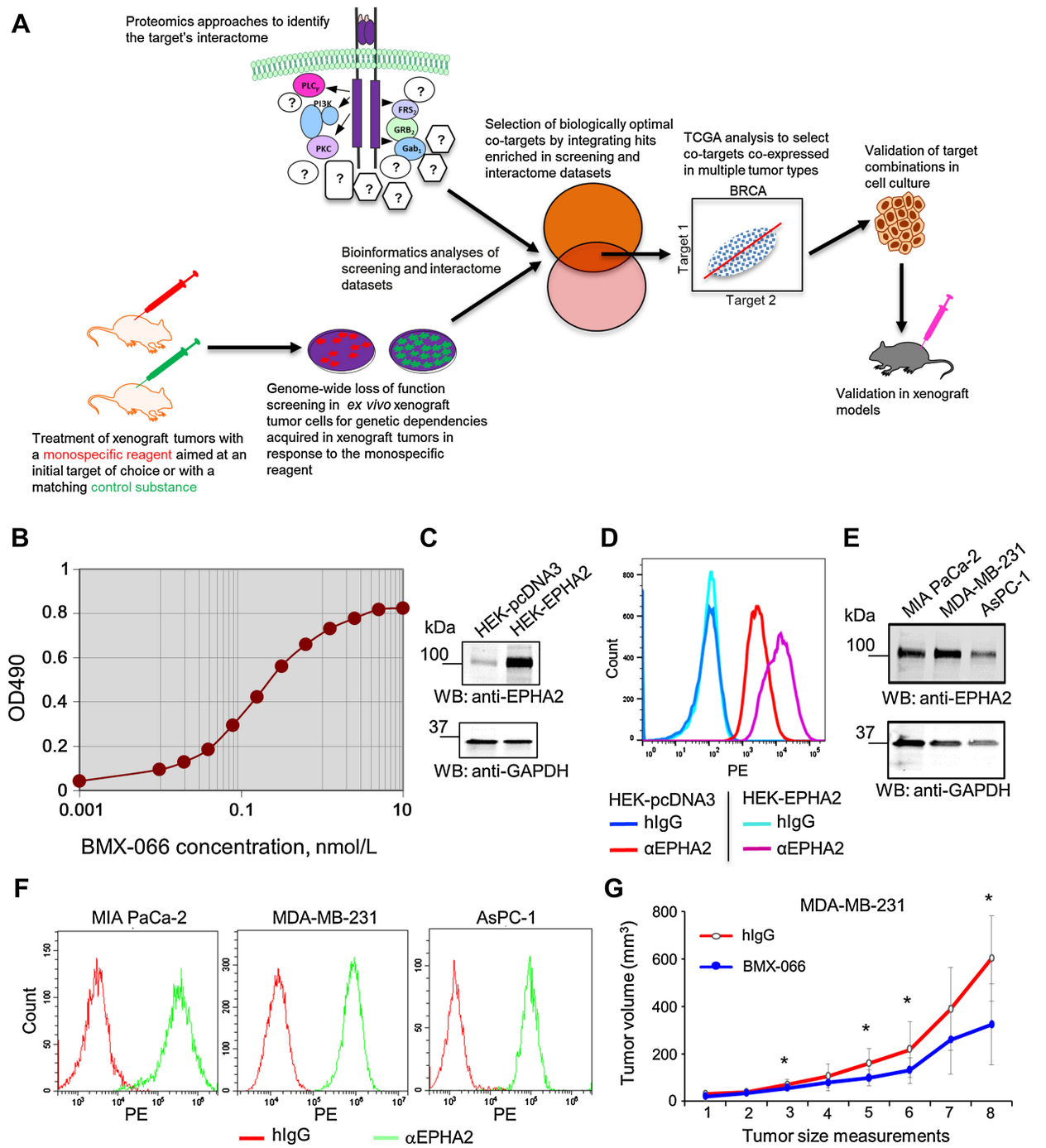

Figure 1.

The roadmap of the proposed unbiased strategy and characterization of the anti-EPHA2 antibody BMX-066. **A,** Workflow for identifying biologically optimal target combinations for bispecific therapeutic reagents. **B,** ELISA analysis of anti-EphA2 antibody (BMX-066) binding to a soluble His-tagged rhEPHA2 protein, representing EPHA2 extracellular portion. BMX-066 was titrated at the indicated concentrations over ELISA plates coated with 100 ng/well of rhEPHA2, and staining was performed with goat anti-human IgG(Fc)-HRP. **C,** Stable expression of EPHA2 in HEK-293 cells transfected with the EPHA2-encoding pcDNA3 expression vector (HEK-EPHA2). Mock-transfected cells (HEK-pcDNA3) are shown as a control. **D,** Flow cytometry analysis of HEK-EPHA2 and HEK-pcDNA3 cells stained with BMX-066 and R-phycoerythrin (PE) conjugated anti-human IgG Fc fragment (anti–hIgG-PE). Staining with nonspecific hIgG was used as a specificity control. **E,** EPHA2 levels in the indicated human cancer cell lines. **F,** Staining of the indicated cancer cells with BMX-066 or nonspecific human IgG (hIgG) and anti–hIgG-PE analyzed by flow cytometry. **G,** Human triple-negative breast cancer cells, MDA-MB-231, were injected into the mammary fat pad region of NOD-SCID mice (1.5–2×10^6 cells/mouse, with equal cell numbers used within each individual experiment). After initial tumor development, mice with detectable tumors were treated with 2 mg/kg of anti–EphA2-BMX, or nonspecific human IgG (hIgG) per week, given in two intraperitoneal injections. Tumor volumes were measured each 3–4 days. The graph summarizes two independent experiments ($n = 11$ for hIgG and $n = 12$ for BMX-066 groups). Data are shown as means ± SD; *, $P < 0.05$, Student t test. Western blotting images were optimized using PowerPoint software where required.

datasets can be accessed at the Gene Expression Omnibus (GEO) database using the accession number GSE171920.

Spearman rank correlation was used to compute the correlation between EGFR and EPHA2 in TCGA patient data. Similarly, the $\log_2$ of RSEM (RNA-Seq Expectation Maximization) normalized expression of EPHA2, EGFR, and c-MET of multiple tissue types as well as Luminal B subtype of breast cancer were extracted from the TCGA patient data and significance was calculated using the non-parametric Wilcoxon rank-sum test between the expression of c-MET and EPHA2. To identify the Luminal B samples, we used the PAM50 signature (9). The BAGEL (Bayesian Analysis of Gene EssentiaLity) algorithm (10) was used to evaluate the quality of the pooled shRNA screen. GSEA (Gene Set Enrichment Analysis) software (11) was used to identify the significantly enriched process of the hits generated from various experiments. A network image was generated using cytoscape software (12), where the top hits from shRNA screen and Bio-ID data were analyzed using GSEA and only hits from the top 15 significantly enriched GO processes with highest normalized enrichment scores were incorporated into the network. We used version 6.2 of the Molecular Signatures Database (MSigDB v 6.2) for GSEAs.

Computational analyses of PDX models

RNA-Seq data and tumor growth parameters of 66 patient-derived xenograft (PDX) models representing non–small cell lung carcinoma (NSCLC) and colorectal cancer treated or not with cetuximab (132 samples total) were curated from the previously published study (13). Only these 132 PDX samples had tumor growth data for cetuximab-treated/untreated conditions. We classified these samples based on the top and bottom quartiles of EPHA2 expression levels (17 PDX models in each category). The AUC of the tumor growth was calculated using Xeva package (v.1.99.20; ref. 14). Following this, we grouped AUC of the NSCLC and colorectal cancer samples into four groups as (i) low expression of EPHA2 with cetuximab treatment; (ii) low expression of EPHA2 in untreated condition; (iii) high expression of EPHA2 with cetuximab treatment, and (iv) untreated with high expression of EPHA2. The AUC of the 4 groups were plotted in boxplots and the significance between the treated conditions of low EPHA2 samples and high EPHA2 samples was calculated using an unpaired non-parametric Kolmogorov–Smirnov test and the P value was found to be 0.0463 ($P < 0.05$).

Surface plasmon resonance

Recombinant human EPHA2 receptor extracellular domain (sEphA2; R&D Systems, #3035-A2–100) was immobilized to the chip ProteOn GLH (Bio-Rad, #176–5013) through amino groups. The measurements were done using Bio-Rad ProteOn XPR36 in 10 mmol/L HEPES, 150 mmol/L NaCl, 0,05% Tween 20, pH 7.4 buffer at 25°C. BMX-066 and BMX-661 were applied at 500 nmol/L concentrations. After washing with the buffer, 100 nmol/L sEGFR (R&D Systems, #1095-ER-002) was applied, as indicated, and after binding saturation, the unbound protein was again washed out.

Dynamic light scattering spectroscopy

Quaternary structure of BMX-661 solution (0.16 mg/mL) in the formulation buffer was measured using Zetasizer Nano ZS spectrometer (Malvern Instruments) at 25°C. The data represent averaged values from three consecutive measurements. The buffer reflection index $n_D = 1.3354$ and buffer dynamic viscosity $\eta = 0.95$ mPa.s at 25°C were measured using latex nanoparticles. For proteins, we used the reflection index $n_D = 1{,}450$ and absorption $\omega = 0.01$. Calculations of protein molecular weight were performed using the Mark–Houwink equation with $K = 7.67 \cdot 10^{-5}$ $sm^2 \cdot s^{-1}$ and $a = 0.428$.

HPLC analyses

Prominence HPLC system from Shimadzu Corporation equipped with UV/Vis detector was used with the size exclusion chromatography column Phenomenox Biosec SEC-s3000 with the exclusion range 5–700 kDa.

Flow cytometry

Cells were stained with indicated mono- or bispecific antibodies and secondary FITC or PE-conjugated anti-human IgG, Fcγ fragment specific. The stained cells were analyzed with Miltenyi Biotec MACSQuant VYB (Miltenyi Biotec Inc.) or Beckman Coulter CytoFLEX (Beckman Coulter) flow cytometers and FlowJo or CytExpert software.

BioID experiments

To assess subcellular enrichment of YFP-BirA*-FLAG or EPHA2-BirA*-FLAG fusion proteins, HEK293 T-Rex cells were pre-fixed with 2% paraformaldehyde (BioShop) for 5 minutes, washed with PBS and fixed with 4% paraformaldehyde for 15 minutes. Cells were permeabilized with 0.2% Triton X-100 (Sigma-Aldrich) for 15 minutes, blocked in 10% goat serum (Wisent) with 0.1% NP-40 (Sigma-Aldrich) in PBS and incubated with rabbit anti-FLAG (Sigma-Aldrich, #F7425) primary antibody in blocking solution for 1 hour. Following 3 washes in PBS with 0.1% NP-40, cells were incubated for 1 hour with Alexa Fluor 488 goat anti-rabbit IgG (Jackson ImmunoResearch, #111–545–003) secondary antibody. Cells were washed 3 times with 0.1% NP-40 in PBS and nuclei were stained with DAPI (Sigma-Aldrich) for 5 minutes. Slides were washed twice with PBS and mounted in ProLong Gold Antifade (Thermo Fisher Scientific). Images were acquired on a confocal laser scanning microscope (Zeiss LSM 700) using Plan-NeoFluar 40x OIL (numerical aperture 1.30) and processed using the ImageJ software.

Cell pellets from four 150-mm dishes were lysed in RIPA buffer (50 mmol/L tris-HCl pH 7.5, 150 mmol/L NaCl, 1 mmol/L EDTA, 1 mmol/L EGTA, 1% NP-40, 0.1% SDS, 0.5% sodium deoxycholate) supplemented with protease inhibitors (1 mmol/L PMSF, 10 $\mu g.mL^{-1}$ aprotinin, 10 $\mu g.mL^{-1}$ leupeptin, and 10 $\mu g.mL^{-1}$ pepstatin) and 250 U of benzonase. Following 1 hour incubation with agitation, lysates were sonicated on ice using three 10 seconds bursts with 2 seconds rest in between and centrifuged 30 minutes at 20,000 × g. Cleared supernatants were further incubated with streptavidin agarose beads (Sigma-Aldrich) for 3 hours with agitation at 4°C. Beads were washed three times with lysis buffer, followed by two washes with 20 mmol/L Tris-HCl (pH 7.4). Proteins were eluted with 50 mmol/L phosphoric acid, three times for 10 minutes and stored at −80°C. Eluted proteins were digested with Promega Sequencing Grade Modified Trypsin (Thermo Fisher Scientific) as described in ref. (15). The resulting peptides were desalted using StageTips (16) and dried down by vacuum centrifugation before LC-MS/MS analyses.

BioID mass spectrometry (MS) and data-dependent acquisition MS analysis

Dried peptides were resuspended in 15 μL of loading solvent (2% acetonitrile, 0.05% TFA), and 5 μL was used for injection onto a 300-μm inner diameter x 5 mm C-18 Pepmap cartridge precolumn (Dionex/Thermo Fisher Scientific) at 20 μL/min in loading solvent. After 5 minutes of desalting, the precolumn was switched online with a 75 μmol/L inner diameter x 50 cm separation column packed with

3 μmol/L ReproSil-Pur C18-AQ resin (Dr. Maisch HPLC GmbH) equilibrated in 95% solvent A (2% acetonitrile, 0.1% formic acid) and 5% solvent B (80% acetonitrile, 0.1% formic acid). Peptides were separated and eluted over a 90 minutes gradient of 5% to 40% solvent B at 300 nL/min flow rate generated by an UltiMate 3000 RSLCnano system (Dionex/Thermo Fisher Scientific) and analyzed on an Orbitrap Fusion mass spectrometer equipped with a nanoelectrospray ion source (Thermo Fisher Scientific). The Orbitrap Fusion was operated in data-dependent acquisition mode with the XCalibur software version 3.0.63 (Thermo Fisher Scientific). Survey MS scans were acquired in the Orbitrap on the 350 to 1,800 m/z range using an automatic gain control (AGC) target of 4e5, a maximum injection time of 50 ms and a resolution of 120,000. The most intense ions per each survey scan were isolated using the quadrupole analyzer in a window of 1.6 m/z and selected for Higher energy Collision-induced Dissociation (HCD) fragmentation with 35% collision energy. The resulting fragments were detected by the linear ion trap at a rapid scan rate with an AGC target of 1e4 and a maximum injection time of 50 ms. Dynamic exclusion was used within a period of 20 seconds and a tolerance of 10 ppm to prevent selection of previously fragmented peptides.

All MS/MS peak lists were generated using Thermo Proteome Discoverer version 2.1 (Thermo Fisher Scientific). MGF sample files were then analyzed using Mascot (Matrix Science; version 2.5.1). Mascot was set up to search UniProt Homo Sapiens database (April 2018 release, 93683 entries) supplemented with "common contaminants" from the Global Proteome Machine (GPM, thegpm.org, July 2017 release) and in house generated BissonN_flags dataset, assuming the digestion enzyme trypsin. Mascot was searched with a fragment ion mass tolerance of 0.60 Da and a parent ion tolerance of 10 ppm. Carbamidomethyl of cysteine was specified as a fixed modification. Oxidation of methionine and phosphorylation of serine, threonine and tyrosine were specified in Mascot as variable modifications. Two miscleavages were allowed. Scaffold (version 4.11.0, Proteome Software Inc.) was used to validate MS-MS–based peptide and protein identifications. Peptide identifications were accepted if they could be established at greater than 91.0% probability to achieve an FDR less than 1.0% by the Scaffold Local FDR algorithm. Protein identifications were accepted if they could be established at greater than 95.0% probability to achieve an FDR less than 1.0% and contained at least 2 identified peptides. Protein probabilities were assigned by the Protein Prophet algorithm (17). Proteins that contained similar peptides and could not be differentiated on the basis of MS-MS analysis alone were grouped to satisfy the principles of parsimony.

Statistical rationale and SAINTexpress analysis for BioID experiments

EPHA2 BioID was performed in biological triplicate and was processed independently on different days using cells from successive passages. YFP-BirA*-FLAG control was treated concomitantly to EPHA2-BirA*-FLAG experimental sample. To minimize carry-over issues during liquid chromatography, extensive washes were performed between each sample. To distinguish background contaminants and non-specific interactions from *bona fide* protein associations, MS data were analyzed with SAINTexpress, a simplified version of the Significance Analysis of INTeractome method (18) via the CRAPome website. The SAINTexpress probability value of each potential protein–protein interaction compared with background contaminants was calculated using default parameters. The three control samples were used in uncompressed mode. The complete list of SAINTexpress analysis results is provided in (Supplementary Table S6). The mass spectrometry proteomics data have been deposited to the ProteomeXchange Consortium via the PRIDE partner repository (19) with the dataset identifier PXD023034 and 10.6019/PXD023034.

Phosphoproteomics experiments

αEPHA2-Cond and cIgG-Tr cells were SILAC labeled in arginine- and lysine-free high glucose DMEM (Caisson Laboratories, DML51–500ML) supplemented with 10% (v/v) dialyzed FBS (Invitrogen, 26400044), and 0.4 mmol/L light arginine and 0.8 mmol/L light lysine for cIgG-Tr cells, or 0.4 mmol/L heavy arginine ($^{13}C_6$, Cambridge Isotopes, CLM-2265-H-PK) and 0.8 mmol/L heavy lysine (D_4, Cambridge Isotopes, DLM-2640-PK) for αEPHA2-Cond cells. Cells were grown at 37°C, 5% CO_2, and until the heavy amino acids were fully incorporated, requiring a month of culturing in SILAC medium.

Single 15-cm petri dish of cells were grown to high confluency, washed with cold 1X PBS three times, scraped to harvest, and boiled in 1% sodium deoxycholate in 50 mmol/L ammonium bicarbonate. The protein concentration was estimated by BCA assay (Pierce, 23227) and 100 μg of protein from each label was mixed, reduced, alkylated, and digested with trypsin (Promega, V5113) as described previously (20). Resulting peptides were cleaned with C-18 STop and Go Extraction (STAGE) tips (21) and eluted peptides were proceeded to lactic acid–modified-TiO_2 enrichment without performing vacuum centrifugation. Equal volume of buffer C consisting of 300 mg/mL DL-lactic acid (Acros Organics, 412965000) in 60% (v/v) acetonitrile and 0.075% (v/v) TFA solution was added to the peptides and passed through two 0.5 mg of bulk TiO_2 beads (GL Sciences, 5010–21315) sitting on C8 STAGE tips (3M, 2214). The tips were then washed with buffer C, and again with buffer B consisting of 80% (v/v) acetonitrile and 0.1% (v/v) TFA, and sequentially eluted with 5% (v/v) NH_4OH and 0.5% (v/v) pyrrolidine. The eluted phosphopeptides were pooled and immediately passed through C18 STAGE tip again and dried with vacuum centrifuge (Eppendorf, Vacufuge) before LC/MS-MS analysis. Three biological replicates were analyzed and each biological replicate was analyzed twice on the LC/MS-MS.

Phosphoproteomics mass spectrometry and data analysis

Each set of cleaned peptides was analyzed by a quadrupole–time of flight mass spectrometer (Impact II; Bruker Daltonics) coupled to an Easy nano LC 1000 HPLC (Thermo Fisher Scientific) using a Captive nanospray ionization source (Bruker Daltonics). The column was constructed in-house and included a fritted 2-cm-long trap column made with 100-μm-inner diameter fused silica and 5-μm Aqua C-18 beads (Phenomenex, 04A-4331) packing material, and a 40–50-cm-long analytic column with an integrated spray tip (6 – 8-μm-diameter opening, pulled on a P-2000 laser puller from Sutter Instruments) made with 75-μm-inner diameter fused silica and 1.9-μm-diameter Reprosil-Pur C-18-AQ beads (Dr. Maisch, r119.aq.0003) packing material. The column was operated at 50°C with an in-house built column heater. Buffer A for the LC consisted of 0.1% (v/v) formic acid, and buffer B for the LC consisted of 0.1% (v/v) formic acid and 80% (v/v) acetonitrile. A standard 90-minute peptide separation was done, and the column was washed with 100% buffer B before re-equilibration with buffer A. The Impact II was set to acquire in a data-dependent auto-MS/MS mode with inactive focus fragmenting the 20 most abundant ions (one at the time at an 18-Hz rate) after each full-range scan from m/z 200 to m/z 2,000 at 5 Hz rate. The isolation window for MS/MS was 2–3 depending on the parent ion mass to charge ratio, and the collision energy ranged from 23 to 65 eV depending on ion mass and charge. Parent ions were then excluded from MS/MS for the next 0.4 minutes and reconsidered whether their

intensity increased more than five times. Singly charged ions were excluded from fragmentation.

Analysis of mass spectrometry data were performed using MaxQuant 1.5.3.30 (22). The search was performed against protein sequences from Uniprot *Homo sapiens* (retrieved on June 13, 2012 with 86,747 entries) plus common contaminants (245 entries) with variable modifications of methionine oxidation, N-acetylation of the proteins, and phosphorylation of serine, tyrosine and threonine in addition to the heavy amino acids used for quantitation and fixed modification of carbamidomethylation of cysteines. The precursor ion mass tolerance was set at 0.006 Da and 40 ppm for fragment ion tolerance. Default match-between-run and requantify parameters were enabled. Data were filtered to 1% FDR at both protein and peptide level based on parallel reverse hits. Phosphoproteomic data are available via ProteomeXchange (ref. 19; http://www.ebi.ac.uk/pride) with identifier PXD023087. Differential expression between αEPHA2-Cond and cIgG-Tr cells was tested using a one-sample *t test* on H/L SILAC ratios. Both the protein group abundance and phosphorylated peptide abundance were tested (*proteinGroups.txt* and *phosphoSites.txt* MaxQuant output tables). Only proteins or phosphosites with at least two H/L SILAC ratios were tested.

Data availability

Data availability for proteomics, Phosphoproteomics, and BioID experiments is described in detail in the related sections of Materials and Methods. Microarray datasets related to the shRNA screens can be accessed at the GEO database using the accession number GSE171920 and access code, "yxarweuenxcbnch." All other data and materials are available upon reasonable requests, BMX-066 and BMX-661—pending their production by Biomirex.

Results

Identification of EGFR as a potential therapeutic partner of EPHA2

Although the EPHA2 receptor contributes to multiple human malignancies, none of the earlier attempts to interfere with its activity has translated into an actual therapy (6). Therefore, to test our strategy for choosing optimal candidates for therapeutic co-targeting (**Fig. 1A**), we selected the EPHA2 receptor as the initial potential target. To identify potential therapeutic partners of EPHA2, we initially screened the Biomirex human phage display Fab library with a repertoire around 4×10^{10} and developed EPHA2-targeting Fab fragments. His6-tagged human EPHA2 extracellular domain (ECD) and EPHA2-Fc construct (murine EPHA2 ECD fused to human IgG Fc fragment) were used for the screening to assure the cross-species reactivity. The selection of cross-reactive anti-EPHA2 Fabs without compromising the selected repertoire was possible due to high degree (83%) of amino acid sequence conservancy between human and mouse EPHA2 ECDs (Supplementary Fig. S1). Eventually, 10 Fabs were converted into human IgG1 mAbs. One of these antibodies, BMX-066, displayed a high affinity against EPHA2 in ELISA assays (**Fig. 1B**). BMX-066 effectively bound EPHA2 recombinantly expressed on the HEK-293 cell membrane and interacted with cancer cells intrinsically expressing this receptor (**Fig. 1C–F**). Administration of BMX-066 partially (by ∼2 fold; $P < 0.05$) suppressed tumor growth in a xenograft model generated with human triple-negative breast cancer (TNBC) cells, MDA-MB-231, in NOD.Cg-Prkdc^{scid} Il2rg^{tm1Wjl}/SzJ (NSG) mice (**Fig. 1G**) and we focused on selecting potential therapeutic partners.

We administered BMX-066 or control non-specific human IgG (cIgG) to NSG mice harboring MDA-MB-231 tumors. Animals were treated for 27 days, tumors were extracted and anti–EPHA2-conditioned (αEPHA2-Cond), and cIgG-treated (cIgG-Tr) *ex vivo* cell populations were established. The biological difference between the αEPHA2-Cond and cIgG-Tr cells was confirmed by comparing their phospho-proteome profiles. This revealed that 160 phosphorylated proteins were differentially expressed and 469 protein phosphorylation events differed significantly between the αEPHA2-Cond and cIgG-Tr cells ($P < 0.05$; **Fig. 2A** and **B**; Supplementary Tables S1 and S2). Specifically, phosphorylated proteins associated with cell/anchoring junction, cell substrate junction and regulation of cell death expressed differently in the αEPHA2-Cond and cIgG-Tr cells, indicating that the αEPHA2-Cond cells indeed represent a biologically distinct *ex vivo* cell population (Supplementary Fig. S2; Supplementary Table S3).

We next used the αEPHA2-Cond and cIgG-Tr cells in a genome-wide shRNA screen with a library containing approximately 90,000 unique shRNAs targeting approximately 18,000 human genes, as we recently described (8), to identify molecules that can be inhibited to selectively eliminate αEPHA2-Cond cells (**Fig. 2C**). A correlation clustergram and density plots of the two screens (αEPHA2-Cond and cIgG-Tr) showed high reproducibility among replicates (Supplementary Fig. S3A and S3B). A high recall of the set of essential genes (indicated by the F measure > 0.7; ref. 23) was achieved in both screens, confirming the high confidence in our analyses (Supplementary Fig. S3C). Overall, we identified 748 statistically significant hits ($P < 0.005$), whose shRNAs dropped out in the αEPHA2-Cond, but not in cIgG-Tr cell populations, indicating that inhibition of these genes should selectively kill anti–EPHA2-treated tumor cells (**Fig. 2D**; Supplementary Table S4). A stringent *P* value cutoff was applied in this analysis to select only the most significant candidates for further investigation. Thus, the shRNA screen identified several cancer-related molecules, including EGFR, SRC, KRAS, NCK1, with an enrichment in cellular processes such as cell death/survival, proliferation, migration, and signal transduction to name a few (**Fig. 2F**; Supplementary Fig. S4, Supplementary Table S5). The selective essentiality of EGFR, SRC, and NCK1 in αEPHA2-Cond cells did make sense, because all these molecules have been shown to be involved in EPHA2-initiated responses (6, 24, 25). Interestingly, EPHA2 suppression was previously reported to elevate KRAS activity (26), suggesting that KRAS overactivation might provide survival advantages to cancer cells in αEPHA2-treated tumors. Therefore, finding it among screening hits was also consistent with earlier observations. These matches between our screening data and previous reports indicated that inhibition of some of these molecules might potentially improve the efficiency of EPHA2 targeting in cancer cells. More importantly for our investigation, capturing these hits provided a strong support for the relevance of our *ex vivo* screening approach.

We expected that integration of genetic and physical interactions of our target should reveal fundamental connections within key functional modules of cancer cells that may become necessary for their survival (27). Therefore, to prioritize candidates among the 748 hits in a completely unbiased manner, we used BioID proteomics to delineate the EPHA2 proximity network. We produced inducible HEK293 T-Rex stable cell lines expressing YFP-BirA*-FLAG (control) or EPHA2-BirA*-FLAG using the Flp-In T-Rex

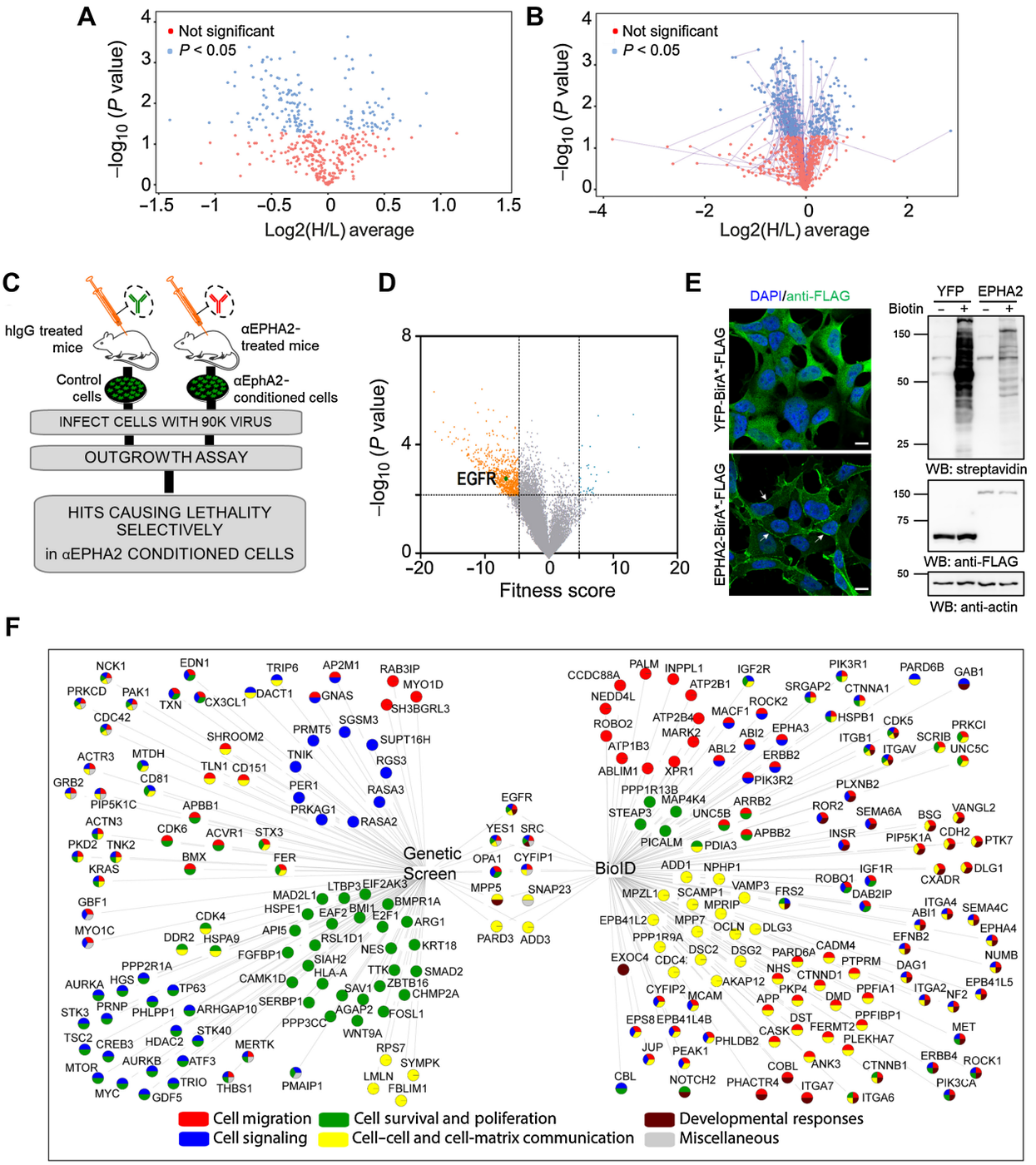

Figure 2.

Identifying potential EPHA2 partners for combination therapies. **A** and **B,** MDA-MB-231 cells were injected into the mammary fat pad region of NSG mice (1.5×10^6 cells/mouse), and mice were treated as in **Fig. 1G** for 27 days. Tumors were extracted, single-cell suspensions were prepared, and *ex vivo* cell cultures were established from BMX-066-conditioned and control hIgG-treated tumors (αEPHA2-Cond and cIgG-Tr cells, respectively). Proteome-wide phosphoprotein (**A**) and phosphopeptide (**B**) analyses revealed significant differences between αEPHA2-Cond and cIgG-Tr cells (shown in blue; *t* test, $P < 0.05$). **C,** The schematic representation of *ex vivo* shRNA-based genome-wide screening strategy for genes that when silenced, selectively suppress αEPHA2-Cond tumor cells. **D,** Volcano plot representing results of genome-wide pooled shRNA screening in αEPHA2-Cond and cIgG-Tr cells. The *x*-axis represents the fitness scores, and the *y*-axis represents negative log of the *P* value. The orange dots represent the hits that, when silenced, significantly ($P < 0.005$) suppress αEPHA2-Cond and not cIgG-Tr cells, whereas inhibition of hits shown in blue provide significant ($P < 0.005$) growth advantage to αEPHA2-Cond cells. **E,** HEK293 T-Rex stable cell lines express EPHA2-BirA*-FLAG bait or a YFP-BirA*-FLAG control. Confocal images display subcellular compartmentalization of BirA* fusion proteins (left; scale bar, 10 μm), and streptavidin Western blotting shows total endogenous protein biotinylation following addition of biotin for 24 hours to the cell culture medium (right). **F,** Cytoscape representation of the hits from the genetic (shRNA) screen and the BioID data that are enriched in multiple gene ontology processes according to the analysis with GSEA software.

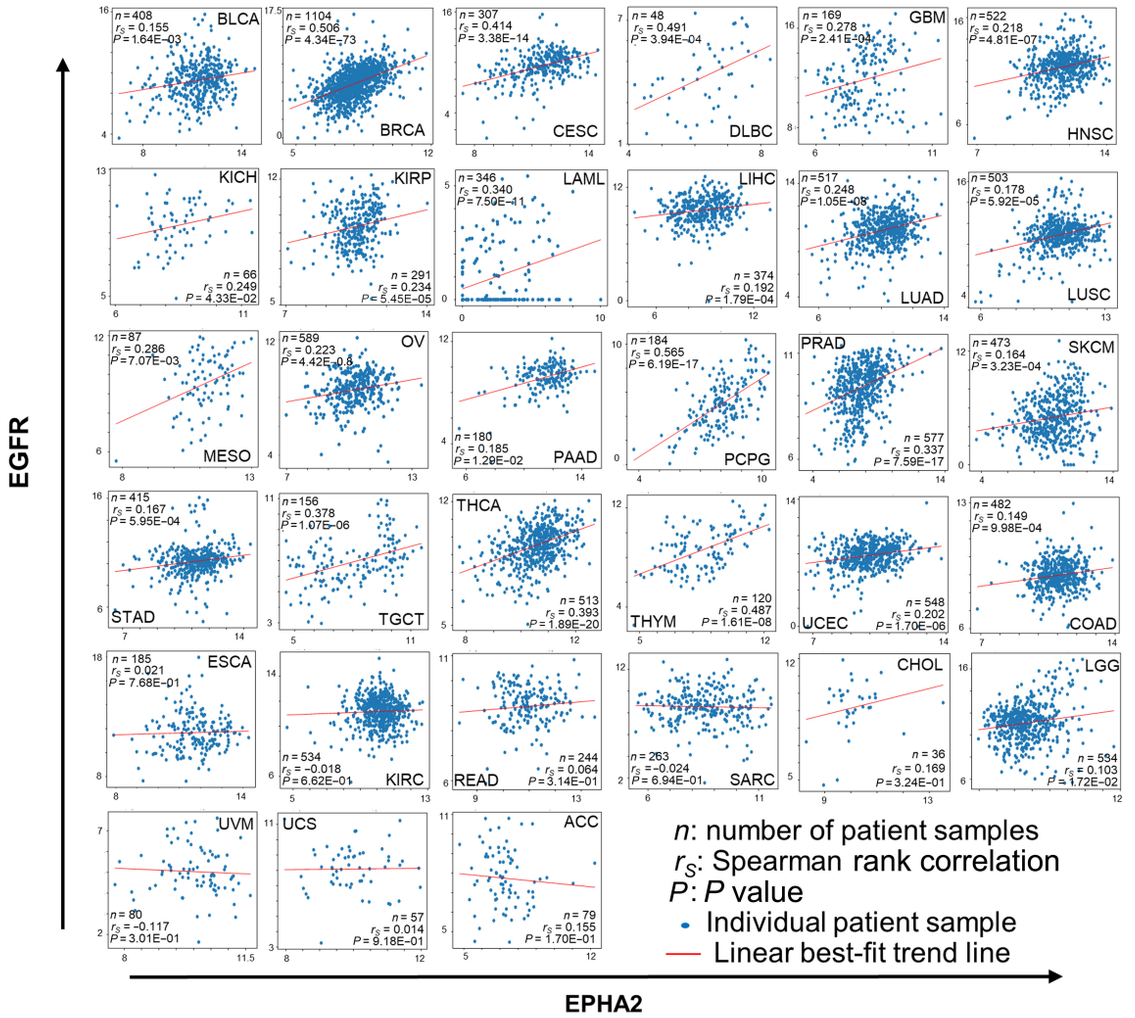

Cancer types:

ACC: Adrenocortical carcinoma
BLCA: Bladder urothelial carcinoma
BRCA: Breast invasive carcinoma
CESC: Cervical squamous cell carcinoma and endocervical adenocarcinoma
CHOL: Cholangiocarcinoma
COAD: Colon adenocarcinoma
DLBC: Lymphoid neoplasm diffuse large B-cell lymphoma
ESCA: Esophageal carcinoma
GBM: Glioblastoma multiforme
HNSC: Head and neck squamous cell carcinoma
KICH: Kidney chromophobe
KIRC: Kidney renal clear cell carcinoma
KIRP: Kidney renal papillary cell carcinoma
LAML: Acute myelogenous leukemia
LGG: Brain lower grade glioma
LIHC: Liver hepatocellular carcinoma
LUAD: Lung adenocarcinoma
LUSC: Lung squamous cell carcinoma
MESO: Mesothelioma
OV: Ovarian serous cystadenocarcinoma
PAAD: Pancreatic adenocarcinoma
PCPG: Pheochromocytoma and paraganglioma
PRAD: Prostate adenocarcinoma
READ: Rectum adenocarcinoma
SARC: Sarcoma
SKCM: Skin cutaneous melanoma
STAD: Stomach adenocarcinoma
TGCT: Testicular germ cell tumors
THYM: Thymoma
THCA: Thyroid carcinoma
UCEC: Uterine corpus endometrial carcinoma
UCS: Uterine carcinosarcoma
UVM: Uveal melanoma

Figure 3.

Co-expression of EPHA2 and EGFR in human tumors. EPHA2 and EGFR expressions in multiple tumor types analyzed using The Cancer Genome Atlas (TCGA) database. The *x*-axis represents the $\log_2$ of RSEM normalized expression of EPHA2, and the *y*-axis represents the $\log_2$ of RSEM normalized expression of EGFR. Each dot in the scatterplots represents individual patient data in the specific cancer type. Included are Spearman rank correlation and lines showing the linear best-fit trend.

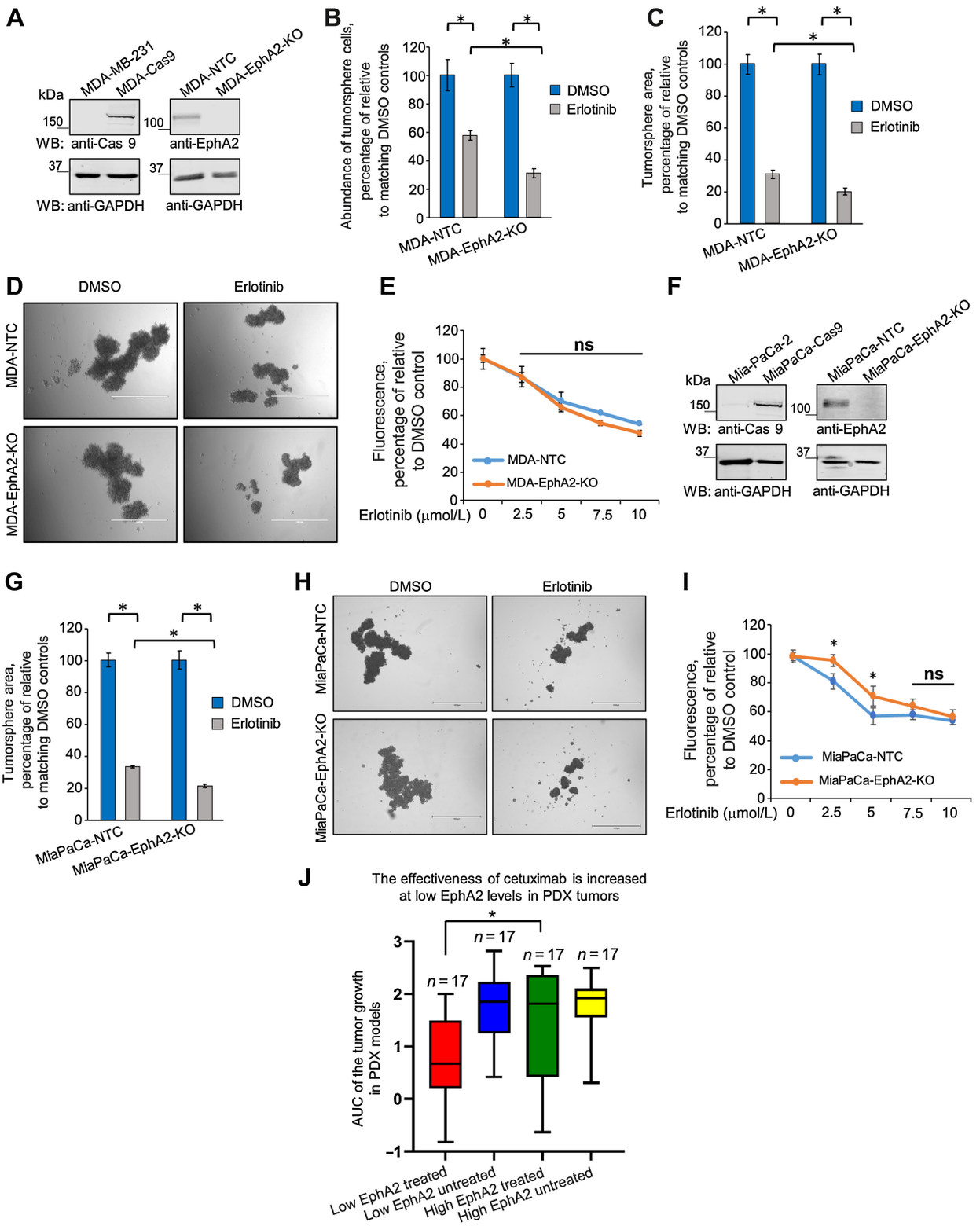
A
MDA-MB-231
MDA-Cas9
MDA-NTC
MDA-EphA2-KO
kDa
150
100
WB: anti-Cas 9
anti-EphA2
37
37
WB: anti-GAPDH
anti-GAPDH
B
Abundance of tumorsphere cells, percentage of relative to matching DMSO controls
DMSO
Erlotinib
MDA-NTC
MDA-EphA2-KO
C
Tumorsphere area, percentage of relative to matching DMSO controls
DMSO
Erlotinib
MDA-NTC
MDA-EphA2-KO
D
DMSO
Erlotinib
MDA-NTC
MDA-EphA2-KO
E
Fluorescence, percentage of relative to DMSO control
ns
MDA-NTC
MDA-EphA2-KO
Erlotinib (μmol/L) 0 2.5 5 7.5 10
F
Mia-PaCa-2
MiaPaCa-Cas9
MiaPaCa-NTC
MiaPaCa-EphA2-KO
kDa
150
100
WB: anti-Cas 9
anti-EphA2
37
37
WB: anti-GAPDH
anti-GAPDH
G
Tumorsphere area, percentage of relative to matching DMSO controls
DMSO
Erlotinib
MiaPaCa-NTC
MiaPaCa-EphA2-KO
H
DMSO
Erlotinib
MiaPaCa-NTC
MiaPaCa-EphA2-KO
I
Fluorescence, percentage of relative to DMSO control
ns
MiaPaCa-NTC
MiaPaCa-EphA2-KO
Erlotinib (μmol/L) 0 2.5 5 7.5 10
J
The effectiveness of cetuximab is increased at low EphA2 levels in PDX tumors
AUC of the tumor growth in PDX models
n = 17
n = 17
n = 17
n = 17
Low EphA2 treated
Low EphA2 untreated
High EphA2 treated
High EphA2 untreated

system (**Fig. 2E**). Addition of biotin to the cell culture medium led to a strong increase in biotinylation of endogenous proteins compared with controls (**Fig. 2E**). We affinity-purified biotinylated proteins following the addition of biotin to YFP-BirA*-FLAG or EPHA2-BirA*-FLAG HEK293, identified them in biological triplicate with MS and eliminated non-specific interactions via SAINTexpress (18), using YFP-BirA*-FLAG-cells as controls. Only high-confidence interactions with a SAINT score ≥0.8, corresponding to a Bayesian FDR (BFDR) ≤2% were considered for analyses. This revealed 420 potential EPHA2 partners (Supplementary Table S6), with several of them predominantly associated with cell–cell and cell–substrate attachment and cell migration (**Fig. 2F**). The Gene Ontology analysis indicated enrichment of 122 of them in at least one of 15 gene sets selected on the basis of top enrichment scores (Supplementary Table S7, Supplementary Fig. S5). Among these proteins, only EGFR was found to be enriched in 14 gene sets (Supplementary Fig. S5), suggesting that it has a strong potential for being involved in the functional cross-talk with EPHA2, especially taking into consideration that EGFR was among the only nine hits found to be enriched in both shRNA screen and BioID assay datasets (**Fig. 2F**).

To further examine the relation between EphA2 and EGFR and its potential clinical relevance, we analyzed the TCGA patient dataset. We found expression levels of EPHA2 and EGFR to positively correlate in multiple if not the majority of malignancies, suggesting that these molecules probably co-operate in cancer cells and should be available for co-targeting in multiple tumor types (**Fig. 3**). This was consistent with previously published data, indicating that EGFR signaling enhances expression of the EPHA2 receptor in cultured cell lines (28, 29). We also assessed the efficiency of the clinically used EGFR inhibitor, erlotinib, in tumorsphere cultures produced by CRISPR-Cas9 *EPHA2* knockout and mock-transduced control MDA-MB-231 cells (**Fig. 4A**). We selected tumorsphere models for these experiments, as tumorspheres better represent tumor biology than cells cultured in monolayers. Interestingly, *EPHA2* knockout significantly increased the sensitivity of tumorsphere cells to erlotinib treatment (**Fig. 4B–D**), while not affecting erlotinib action in cancer cell monolayers (**Fig. 4E**), once again highlighting biological differences between tumorspheres and cells in 2-D cultures. Similar effects of *EPHA2* knockout were also observed in pancreatic cancer MIA PaCa-2 cells (**Fig. 4F–I**). Moreover, our analysis of EPHA2 expression in 66 previously described independent PDX models of colorectal cancer and NSCLC (13) revealed that treatment with the therapeutic anti-EGFR antibody, cetuximab, is significantly ($P < 0.05$, Kolmogorov–Smirnov test) more effective in tumors with low EPHA2 levels (**Fig. 4J**). This finding was consistent with our observations in tumorspheres and agreed well with a recently published report, showing that the EPHA2–EGFR crosstalk contributes to the aggressiveness of both colon and lung cancers (30). Similarly, earlier data indicate that *EPHA2* silencing can suppress lung cancer cells that developed resistance to EGFR inhibitor, erlotinib (31), and that lower EPHA2 levels correlate with better responsiveness of colorectal cancer patients to cetuximab (32, 33).

Overall, a prediction based on the integration of genetic and proteomics approaches with gene expression analyses of the TCGA database was successfully validated by subsequent *EPHA2* knockout experiments, and analyses of independently reported PDX models. This prediction clearly pointed toward EGFR as a potential therapeutic co-targetable partner of EPHA2.

Generation and characterization of the bispecific anti-EGFR/EPHA2 antibody

To co-target EPHA2 and EGFR and assure a synchronized delivery of anti-EPHA2 and anti-EGFR reagents to tumor cells, we generated a

Figure 4.

Co-suppression of EPHA2 and EGFR enhances elimination of cancer cells. **A,** MDA-MB-231 were transduced with the CAS9-encoding pLv5 lentiviral vector (MDA-Cas9), subjected to selection with blasticidin, and CAS9 expression was assessed by Western blot (left). MDA-Cas9 cells were transduced with LV04 lentiviral vectors from Sanger human CRISPR library encoding EphA2-targeting sgRNAs, ID 2400992 and ID 2400602 (MDA-EphA2-KO) or control, non-targeting sgRNA Lenti CRISPR Universal Non-Target Control #2 Plasmid (LV04 vector; MDA-NTC) and subjected to puromycin selection. *EPHA2* knockout was confirmed by Western blot (right). **B,** MDA-EphA2-KO and control cells were seeded at 1.6×10^3 cells per well (three wells per condition) in the MamoCult Basal Medium (Stemcell Technologies, Cat # 05621) into ultralow attachment 24-well plates and allowed to form tumorspheres for 8 days in the presence of 10 μmol/L of erlotinib or a matching concentration of DMSO. Tumorspheres in each well were trypsinized and individual cells counted. The graph represents abundance of the erlotinib-treated cells as percentages relative to matching DMSO controls. **C,** The indicated cells were seeded and allowed to form tumorspheres as in (**B**). Images of tumorspheres in each well were taken using an EVOS m5000 imager, and overall tumorsphere area was summarized using ImageJ software. The graph represents tumorsphere area of erlotinib-treated cells as a percentage of relative to the area in a matching DMSO control. **D,** Representative images of erlotinib-treated and DMSO-treated tumorspheres formed by MDA-EphA2-KO and MDA-NTC cells; scale bar, 1,000 μm. **E,** The indicated cells were seeded in DMEM medium with 1% FBS at 4.5×10^3 cells per well (five wells per condition) into 96-well plates to form monolayer cultures. Cells were treated for 72 hours with the indicated concentrations of erlotinib or DMSO concentration matching DMSO volume loaded with the highest erlotinib dose. Cell survival was quantified using the resazurin assay (R&D Systems, Cat# AR002). The graph represents survival of erlotinib-treated cells as percentages relative to matching DMSO controls. **F,** CAS9 was expressed in MIA PaCa-2 cells (MiaPaCa-Cas9) and *EPHA2* knocked out (MiaPaCa-EphA2-KO) as in (**A**). Nontargeting sgRNA was used as a control (MiaPaCa-NTC), and CAS9 expression and *EPHA2* knockout were confirmed by Western blot. **G,** The effect of erlotinib on tumorspheres formed by MiaPaCa-EphA2-KO and MiaPaCa-NTC cells was examined as in (**C**); cell seeding was done at 1×10^3 cells/well into ultralow attachment 24-well plates. Tumorsphere cell counting (as in **B**) was not performed, as we could not get single-cell suspensions from these tumorspheres without damaging cells. **H,** Representative images of tumorspheres formed by the indicated cells in the presence of 10 μmol/L of erlotinib or matching DMSO control; scale bar, 1,000 μm. **I,** MiaPaCa-EphA2-KO and MiaPaCa-NTC cells were treated with erlotinib or DMSO in monolayer cultures, and cell survival was analyzed as in (**E**). **J,** Analysis of the AUC of PDX models representing non–small cell lung carcinoma and colorectal cancer. PDX models treated or not with cetuximab were classified on the basis of EPHA2 expression levels (top and low quartiles). The analysis reveals significantly stronger reduction in tumor size in response to cetuximab treatment in models with low EPHA2 levels compared with tumors with high EPHA2 expression. *, $P < 0.05$, Kolmogorov–Smirnov test. Data from monolayer (**E** and **I**) and tumorsphere (**B**, **C**, and **G**) experiments were analyzed using the Student *t* test, *, $P < 0.01$. Western blot images were optimized using PowerPoint software where required.

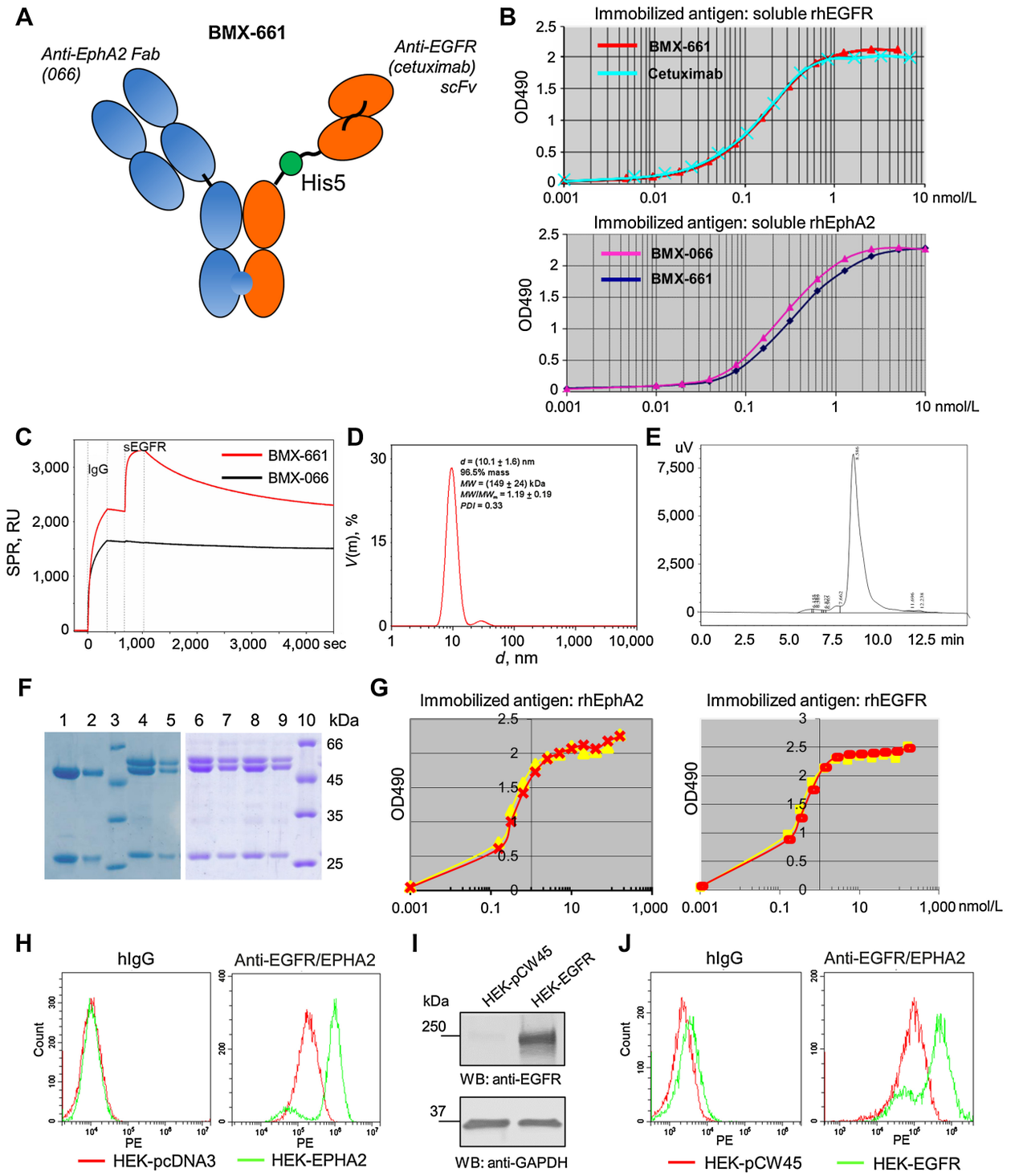

Figure 5.

Structure and characterization of the bispecific anti-EGFR/EPHA2 antibody. **A,** An asymmetric monovalent bispecific anti-EphA2/EGFR antibody, BMX-661, composed of Fab fragment of BMX-066 and scFv derived from the anti-EGFR antibody cetuximab, fused to the human IgG1 Fc domain. Fc fragments of the antibody are heterodimerized by knob-in-hole mutations in the CH3 domains of the heavy chains. His5 amino acid tag is incorporated into the linker between scFv and the Fc region for purification purposes. **B,** Binding of BMX-661 and cetuximab to soluble immobilized rhEGFR (extracellular portion, top) or BMX-661 and BMX-066 to immobilized rhEPHA2 (bottom) in the ELISA assay. (*Continued on the following page.*)

bispecific anti-EGFR/EPHA2 antibody. The antibody, BMX-661, was heterodimerized through the "Knob-Hole" approach using BMX-066 and cetuximab, where the amino acids of heavy chains CH3 domains were remodeled with "knob-into-holes" mutations (34). One arm of BMX-661 was composed of BMX-066–derived Fab, whereas another part was made by the fusion of VH and VL domains of cetuximab using the (G4S)3 linker to form scFv. To assist bioanalytics and purification, the non-immunogenic His5 tag (35) was incorporated between cetuximab scFv and Fc (**Fig. 5A**). BMX-661 was expressed in CHO-S cells and purified using Protein A followed by Ni^{+}-resins. Its affinities to EPHA2 and EGFR were measured by ELISA, and proved to be similar for both antibody arms (**Fig. 5B**). Surface plasmon resonance measurements also confirmed that there is no steric hindrance between the anti-EPHA2 and anti-EGFR arms of BMX-661 in binding to their corresponding antigens (**Fig. 5C**).

BMX-661 was additionally characterized in several conventional bioanalytical assays, including dynamic light scattering (**Fig. 5D**), HPLC (**Fig. 5E**), and SDS-PAGE (**Fig. 5F**), which confirmed good aggregation, thermal and proteolytic characteristics. It remained stable at 5 mg/mL for up to 200 days at 4°C and three days at 37°C (**Fig. 5F**), although some batches were observed to lose activity after longer storage at 4°C or room temperature. The antibody was also stable in human blood serum, as determined by its incubation for seven days at 37°C followed by the assessment of its binding characteristics to EPHA2 and EGFR (**Fig. 5G**). BMX-661 recognized EGFR and EPHA2 on the cell membrane (**Fig. 5H–J**), and interacted with EPHA2- and EGFR–co-expressing cancer cells (**Fig. 6A** and **B**). Overall, the bioanalytical characterization of BMX-661 highlighted its potential for preclinical and clinical testing.

To assess therapeutic properties of BMX-661, we tested it in xenograft models of human malignancies. To examine its effect on tumor growth and metastasis, we exploited as in **Fig. 1G**, MDA-MB-231 cells that metastasize into lungs (36). MDA-MB-231 cells stably expressing EGFP were used to develop tumors in mammary fat pads of NSG mice. Tumors were allowed to grow to a measurable size and the mice were treated with BMX-661. This very effectively, by up to approximately 4-fold (t test, $P < 0.05$), inhibited tumor growth and strongly suppressed metastasis into lungs, demonstrating both antitumor efficiency and anti-metastatic action of BMX-661 (**Fig. 6C**). Targeted treatment approaches are usually most effective, when applied in combinations with traditional chemotherapies and when applied at a lower dose, BMX-661 proved to enhance the therapeutic action of a DNA-damaging drug cisplatin in MDA-MB-231 xenografts (**Fig. 6D**). The antitumor activity of BMX-661, was also tested in the HCI-010 PDX that represents TNBC and closely mimics properties of the original tumor (37). Excitingly, treatment with BMX-661 strongly suppressed tumors in this model (**Fig. 6E**). The therapeutic effect was not restricted to TNBC, because BMX-661 administration also significantly inhibited tumor growth in a xenograft model representing pancreatic cancer (**Fig. 6F**).

Taken together, these data convincingly confirmed that EGFR is the molecule of choice for co-targeting with EPHA2 in tumor cells and highlighted the potential of our unbiased strategy for selecting efficient target combinations for bispecific therapeutic reagents.

Discussion

Accumulating advances in the understanding of the molecular machinery responsible for tumor development have triggered the generation of multiple therapeutic approaches that target individual components of cancer-promoting mechanisms. These treatments depend on the development of selective small-molecule inhibitors and therapeutic antibodies (38, 39). Unfortunately, tumors expressing matching targets often produce low responses or acquire resistance to these compounds, leading to relapse. This is at least in part driven by the innate tumor heterogeneity, which allows survival of treatment-resistant cancer cell populations (1, 40). One of the strategies of choice for minimizing cancer resistance is the development of selective dual-specificity regents, which are currently mostly represented by bispecific antibodies aimed at two different oncogenic cell surface molecules (41–43). The bispecific nature of these therapeutics allows perfectly synchronized action on both targets, optimizing tumor-suppressing efficiency, tumor targeting, and minimizing the evolutionary potential of cancer cells. The relevance of this notion is illustrated by our data, showing that high expression of two pro-malignant RTKs, EGFR and

(*Continued.*) Soluble antigen proteins (2 μg/mL) were immobilized onto ELISA plates, and after incubation with the indicated concentrations of BMX-661, BMX-066, or cetuximab, bound antibodies were detected with goat anti-human IgG(Fc)-HRP. **C,** The surface plasmon resonance–binding curves for BMX-066 and BMX-661. Soluble rhEPHA2 was immobilized onto the ProteOn GLH chip through amino groups in the 150 mmol/L NaCl, 10 mmol/L HEPES pH 7.4, 0.05% Tween-20 buffer. After washing out the unbound protein, BMX-066 and BMX-661 were applied at 500 nmol/L (IgG) and the unbound antibodies were removed with the buffer. Following this, rhEGFR was introduced, as indicated (sEGFR), and the unbound ligand was removed after binding saturation. The measurements were done using Bio-Rad ProteOn XPR36, at 25°C. Bispecific BMX-661 bound both immobilized rhEPHA2 and soluble rhEGFR, whereas, as expected, monospecific anti–EPHA2 BMX-066 did not interact with rhEGFR. **D,** Dependence of integral volume of particles, V, from their sizes, d, for BMX-661 preparation measured by dynamic light scattering. BMX-661 (0.16 mg/mL) was analyzed in the 20 mmol/L L-histidine, 30 mmol/L citric acid, 32 mmol/L Na_2HPO_4, 1% trehalose, 0.05% Tween-20; pH = 6.0 buffer. The content of multimeric forms of the MABs was estimated using spectrometer ZS Zetasizer Nano (Malvern Instruments) at 25°C. **E,** HPLC analysis of BMX-661 solution, size exclusion chromatography. **F,** Stability of BMX-661 estimated by SDS-PAGE under reducing conditions. Freshly isolated antibodies BMX-066 (lanes 1 and 2) and BMX-661 (lanes 4 and 5); BMX-661 stored for 200 days at 4°C (lanes 6 and 7) or incubated at 37°C for 3 days (lanes 8 and 9) in the formulation buffer were loaded at 11 (lanes 1, 4, 6, and 8) and 4 (lanes 2, 5, 7, and 9) micrograms per well. Lanes 3 and 10 molecular weight markers. The top band in the heavy chain region of BMX-661 represents the EGFR-binding scFV-Fc portion of the antibody, whereas the second band and the lower band represent heavy and light chains of the EPHA2-binding portion of bispecific antibody. **G,** Blood serum stability of BMX-661. ELISA titration curves before (yellow) and after (red) incubation of 2 mg/mL of BMX-661 in human blood serum (Sigma-Aldrich, Cat # H4522) for 7 days at 37°C. ELISA plates were coated with rhEPHA2 (left panel) or sEGFR (right), and blood serum samples with BMX-661 were applied to titration. Staining was performed with goat anti-human IgG(Fc)-HRP. **H,** Flow cytometry analysis of BMX-661 with HEK-EPHA2 and HEK-pcDNA3 cells. Anti-hIgG-PE was used as a secondary antibody. Staining with nonspecific hIgG was used as a specificity control. **I,** EGFR levels in HEK-293 cells stably transfected with the EGFR-encoding pCW45 expression vector (HEK-EGFR) or mock-transfected HEK-293 (HEK-pCW45). **J,** Flow cytometry analysis of BMX-661 with HEK-EGFR and HEK-pCW45 cells. Western blot images were optimized using PowerPoint software where required.

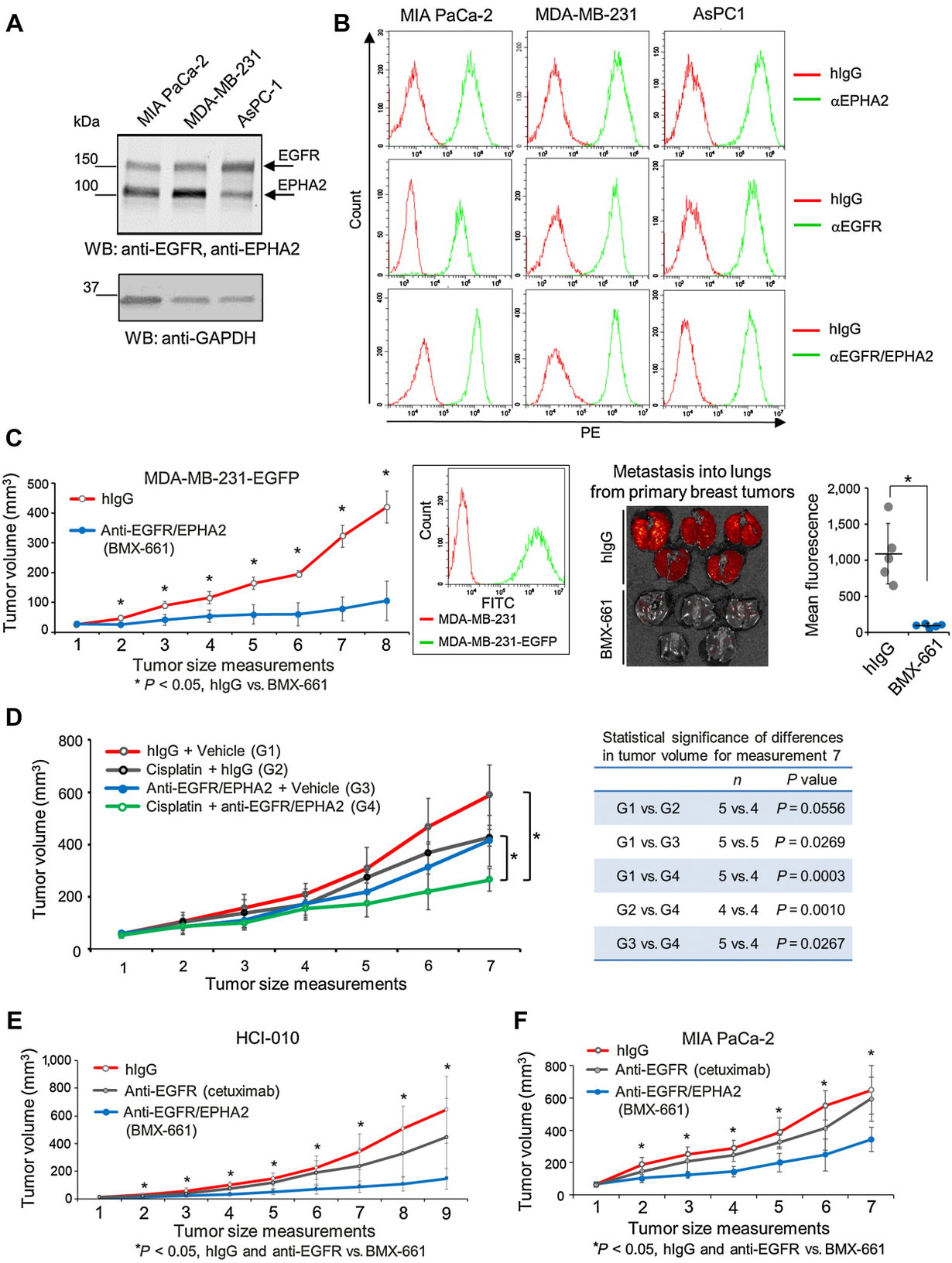
A
MIA PaCa-2
MDA-MB-231
AsPC-1
kDa
150
100
EGFR
EPHA2
WB: anti-EGFR, anti-EPHA2
37
WB: anti-GAPDH
B
MIA PaCa-2
MDA-MB-231
AsPC1
hIgG
αEPHA2
hIgG
αEGFR
hIgG
αEGFR/EPHA2
Count
PE
C
MDA-MB-231-EGFP
hIgG
Anti-EGFR/EPHA2
(BMX-661)
Tumor volume (mm3)
Tumor size measurements
* P < 0.05, hIgG vs. BMX-661
Count
FITC
MDA-MB-231
MDA-MB-231-EGFP
Metastasis into lungs
from primary breast tumors
hIgG
BMX-661
Mean fluorescence
hIgG
BMX-661
D
hIgG + Vehicle (G1)
Cisplatin + hIgG (G2)
Anti-EGFR/EPHA2 + Vehicle (G3)
Cisplatin + anti-EGFR/EPHA2 (G4)
Tumor volume (mm3)
Tumor size measurements
Statistical significance of differences in tumor volume for measurement 7
n
P value
G1 vs. G2 5 vs. 4 P = 0.0556
G1 vs. G3 5 vs. 5 P = 0.0269
G1 vs. G4 5 vs. 4 P = 0.0003
G2 vs. G4 4 vs. 4 P = 0.0010
G3 vs. G4 5 vs. 4 P = 0.0267
E
HCI-010
hIgG
Anti-EGFR (cetuximab)
Anti-EGFR/EPHA2
(BMX-661)
Tumor volume (mm3)
Tumor size measurements
*P < 0.05, hIgG and anti-EGFR vs. BMX-661
F
MIA PaCa-2
hIgG
Anti-EGFR (cetuximab)
Anti-EGFR/EPHA2
(BMX-661)
Tumor volume (mm3)
Tumor size measurements
*P < 0.05, hIgG and anti-EGFR vs. BMX-661

EPHA2, coincides in multiple malignancies (**Fig. 3**), which suggests that their co-targeting with bispecific reagents is likely to produce beneficial therapeutic effects. Indeed, more than 50 bispecific antibodies have already reached clinical trials (43). Most recently, the anti-EGFR/c-MET antibody, amivantamab, has been fast-tracked into clinics by Janssen (44) https://www.fda.gov/drugs/resources-information-approved-drugs/fda-grants-accelerated-approval-amivantamab-vmjw-metastatic-non-small-cell-lung-cancer and two similar bispecific anti-EGFR/c-MET antibody programs have been successfully developed by Eli Lilly (45) and Merck KGaA (46).

Until now, target combinations for bispecific reagents have been mostly chosen on the basis of the pre-existing knowledge of functions of cancer-related molecules, which may often result in suboptimal tumor-suppressing properties (1–3). To address this, we suggest a systematic and completely unbiased strategy for designing bispecific therapeutics. Thus, to identify optimal candidates for co-targeting, we suggest to pre-condition cancer cells in xenograft tumors to the action of a mono-specific reagent aimed at the selected candidate target. These pre-conditioned cells can be subsequently used *ex vivo*, in genome-wide loss of function screening to identify acquired dependencies. Cross-referencing the genetic dependencies with the delineated physical target's interactome should reveal key functional connections essential for cancer cell survival. The final selection of the biologically optimal co-target is based on the unrestricted bioinformatics analysis of the TCGA database, to assure that the chosen combination of molecules occurs at a significant frequency in human malignancies and therefore, should have a high level of therapeutic relevance. In our investigation, this strategy pointed toward two RTKs, namely EPHA2 and EGFR as an optimal combination for co-targeting. Remarkably, this prediction was consistent with previous findings that reported a functional crosstalk between EPHA2 and EGFR in cancer cells and implicated EPHA2 in the resistance to EGFR inhibitors in some malignancies, including colorectal cancer and non-NSCLC (24). The close match between our prediction and previous independent reports highlights the high level of accuracy of our unbiased strategy. It also suggests that additional potential target combinations can be identified with a high level of confidence using our coordinated genome-wide/proteome-wide data (Supplementary Tables and **Fig. 2F**).

To further validate our prediction, we have generated and characterized a human anti-EGFR/EPHA2 antibody, BMX-661. As anticipated, BMX-661 very efficiently suppressed aggressive TNBC and pancreatic cancer tumors in xenograft models, when compared with its prototypic anti-EGFR antibody, cetuximab. BMX-661 proved to be effective in xenograft cancer models at a relatively low dose of 2 mg/kg/wk compared with doses exceeding 15 mg/kg/wk often used for testing RTK-targeting antibodies for therapeutic efficiency (47–49). When applied at an even lower dose of 1.5 mg/kg/wk, BMX-661 worked well in combination with cisplatin and significantly improved the antitumor action of this conventional chemotherapeutic drug. Although the exact mechanism of BMX-661 action is still being dissected, its clinical potential is highlighted by our data, showing that targets for BMX-661 are co-expressed in multiple human malignancies and that the antibody produces strong antitumor responses. Currently, monospecific EGFR-inhibiting reagents are efficient in only a few malignancies and inflict incomplete therapeutic effects (50–52). We expect BMX-661 to improve the therapeutic effectiveness of EGFR inhibition in a variety of cancers expressing both antigens. Thus, co-suppressing EGFR and c-MET has a high therapeutic potential (44), and our work indicates that co-targeting EGFR and EPHA2 would provide a very effective complementary treatment approach. This could be especially relevant in EGFR-expressing tumors with EPHA2 levels similar or higher compared with c-MET (Supplementary Fig. S6), suggesting a need for further preclinical evaluation in matching models.

Importantly, our work with BMX-661 demonstrates the feasibility of our multipronged unbiased strategy for selecting optimal co-targets for combination therapies and for supporting generation of efficient bispecific therapeutic reagents. We certainly realize that this strategy relies on the accurate choice of the first target for a combination treatment, and also on several advanced approaches that require sufficient resources and expertise. That said, we also believe that current rapid advances in research technologies and in the understanding of cancer biology should allow to effectively use our approach in a broad variety of drug development projects.

Authors' Disclosures

I. Alexandrov reports a patent for antibody pending. B. Wang reports grants from NIH during the conduct of the study. B.M. Toosi reports nonfinancial support from Biomirex Inc. during the conduct of the study. N. Bisson reports grants from FRQNT during the conduct of the study. T.A. Mirzabekov reports a patent for bispecific anti-EGFR/anti-EphA2 antibody pending; in addition, T.A. Mirzabekov reports employment as chief executive officer and president of Biomirex, Inc., which owns the anti-EGFR/anti-EphA2 bispecific antibody.

Figure 6.

BMX-661 suppresses tumors in xenograft models. **A,** EGFR and EPHA2 levels in the indicated human malignant cell lines. **B,** Flow cytometry analysis of BMX-661 with the indicated cell lines. **C,** Xenograft tumors were developed in NSG mice by injecting MDA-MB-231 cells stably expressing EGFP, as described previously in **Fig. 1G**. Flow cytometry inset shows EGFP expression in MDA-MB-231. Tumors were allowed to achieve a measurable size, and mice were treated by twice weekly intraperitoneal injections of BMX-661 or nonspecific hIgG ($n = 5$ per treatment). Tumor growth was monitored as in **Fig. 1G**, and upon experiment termination, lungs were extracted and imaged with the IVIS Spectrum CT Imaging System to assess metastasis. Fluorescence is shown in red; contrast was adjusted in PowerPoint to optimize the image. The graph on the right represents the mean fluorescence intensity of lungs in each group as quantified for the total surface area of each sample using Living Image software. **D,** MDA-MB-231 cells were injected into the mammary fat pad of NSG mice (1.5×10^6 cells/mouse) as in **Fig. 1F**. Mice with measurable tumors were randomly assigned into four groups (G1–G4) and treated with intraperitoneal injections of BMX-661 (1.5 mg/kg/wk, split into two injections 3–4 days apart), cisplatin (2.5 mg/kg/wk), a combination of both, or a nonspecific human IgG and a solvent control matching cisplatin solvent (PBS) in a 2×2 design. Tumor growth was monitored as in **Fig. 1G**. **E,** Triple-negative breast cancer patient-derived xenograft cells, HCI-010, were introduced into the mammary fat pad region of 4- to 6-week-old female NSG mice (1×10^6 cells per mouse), and tumors were allowed to develop to a measurable size. The mice were treated intraperitoneally twice a week by 1 mg/kg injection of hIgG, cetuximab, or BMX-661, and tumor growth was monitored as in **Fig. 1G**. The graph summarizes three independent experiments ($n = 14$ per group). **F,** MIA PaCa-2 cells were mixed with Corning Matrigel Matrix (4×10^6 cells in 50 μL of PBS mixed with 50 μL of the Matrigel) and injected subcutaneously into the right flanks of 5- to 6-week-old NSG male mice. Once tumors reached a measurable size, mice were treated twice a week by intraperitoneal injections of 1 mg/kg of hIgG, cetuximab or BMX-661. Tumor growth was monitored as in **Fig. 1G**. The graph summarizes two independent experiments ($n = 10$ for hIgG, and $n = 11$ for anti-EGFR and anti-EGFR/EPHA2–treated groups). Western blot images were optimized using PowerPoint software where required. Data in the graphs are shown as means ± SD; *, $P < 0.05$, treatment with hIgG and cetuximab versus BMX-661, Student *t* test.

F.J. Vizeacoumar reports nonfinancial support from Biomirex Inc. during the conduct of the study. A. Freywald reports nonfinancial support from Biomirex Inc. during the conduct of the study; in addition, A. Freywald reports an advisory role on the scientific board of Biomirex Inc., which is a volunteer/public service activity to support the development of new cancer therapies for which A. Freywald has received no compensation. No disclosures were reported by the other authors.

Authors' Contributions

A. El Zawily: Investigation, methodology. **F.S. Vizeacoumar:** Data curation, investigation, methodology. **R. Dahiya:** Investigation, methodology. **S.L. Banerjee:** Data curation, investigation, methodology. **K.K. Bhanumathy:** Investigation, methodology. **H. Elhasasna:** Investigation, methodology. **G. Hanover:** Investigation, methodology. **J.C. Sharpe:** Investigation, methodology. **M.G. Sanchez:** Investigation, methodology. **P. Greidanus:** Investigation, methodology. **R.G. Stacey:** Data curation, investigation, methodology. **K.-M. Moon:** Investigation, methodology. **I. Alexandrov:** Investigation, methodology. **J.P. Himanen:** Investigation, writing–review and editing. **D.B. Nikolov:** Investigation, writing–review and editing. **H. Fonge:** Investigation, writing–review and editing. **A.P. White:** Investigation, methodology. **L.J. Foster:** Investigation, methodology, writing–review and editing. **B. Wang:** Conceptualization, writing–review and editing. **B.M. Toosi:** Conceptualization, validation, methodology, writing–original draft, writing–review and editing. **N. Bisson:** Conceptualization, investigation, methodology, writing–original draft, writing–review and editing. **T.A. Mirzabekov:** Conceptualization, investigation, methodology, writing–original draft, writing–review and editing. **F.J. Vizeacoumar:** Conceptualization, funding acquisition, writing–original draft, writing–review and editing. **A. Freywald:** Conceptualization, funding acquisition, writing–original draft, writing–review and editing.

Acknowledgments

We thank Dr. A.L. Welm, Co-Director, Cell Response and Regulation Program, Huntsman Cancer Institute, University of Utah, for providing the HCI-010 PDX and for the related technical advice. This work was supported by the Canadian Institutes of Health Research grants (PJT-156401; PJT-156309); College of Medicine, University of Saskatchewan, and Be Like Bruce funding (to A. Freywald and F.J. Vizeacoumar); and Genome Canada (264PRO; to L.J. Foster). R. Dahiya was supported by an SHRF fellowship; F.S. Vizeacoumar is supported by the College of Medicine, University of Saskatchewan; and G. Hanover, M.G. Sanchez, and H. Elhasasna were supported by CoMGRAD awards, College of Medicine, University of Saskatchewan.

The publication costs of this article were defrayed in part by the payment of publication fees. Therefore, and solely to indicate this fact, this article is hereby marked "advertisement" in accordance with 18 USC section 1734.

Note

Supplementary data for this article are available at Clinical Cancer Research Online (http://clincancerres.aacrjournals.org/).

Received September 9, 2022; revised December 26, 2022; accepted March 1, 2023; published first March 28, 2023.

References

1. Marusyk A, Janiszewska M, PKI Heterogeneity. The Rosetta stone of therapy resistance. Cancer Cell 2020;37:471–84.
2. Tsimberidou AM, Fountzilas E, Nikanjam M, Kurzrock R. Review of precision cancer medicine: evolution of the treatment paradigm. Cancer Treat Rev 2020;86:102019.
3. Chen SH, Lahav G. Two is better than one; toward a rational design of combinatorial therapy. Curr Opin Struct Biol 2016;41:145–50.
4. Paul JM, Templeton SD, Baharani A, Freywald A, Vizeacoumar FJ. Building high-resolution synthetic lethal networks: a "Google map" of the cancer cell. Trends Mol Med 2014;20:704–15.
5. Zafra F, Piniella D. Proximity labeling methods for proteomic analysis of membrane proteins. J Proteomics 2022;264:104620.
6. Wilson K, Shiuan E, Brantley-Sieders DM. Oncogenic functions and therapeutic targeting of EphA2 in cancer. Oncogene 2021;40:2483–95.
7. Cheever MA, Allison JP, Ferris AS, Finn OJ, Hastings BM, Hecht TT, et al. The prioritization of cancer antigens: a national cancer institute pilot project for the acceleration of translational research. Clin Cancer Res 2009;15:5323–37.
8. Paul JM, Toosi B, Vizeacoumar FS, Bhanumathy KK, Li Y, Gerger C, et al. Targeting synthetic lethality between the SRC kinase and the EPHB6 receptor may benefit cancer treatment. Oncotarget 2016;7:50027–42.
9. Netanely D, Avraham A, Ben-Baruch A, Evron E, Shamir R. Expression and methylation patterns partition luminal-A breast tumors into distinct prognostic subgroups. Breast Cancer Res 2016;18:74.
10. Hart T, Moffat J. BAGEL: a computational framework for identifying essential genes from pooled library screens. BMC Bioinf 2016;17:164.
11. Subramanian A, Tamayo P, Mootha VK, Mukherjee S, Ebert BL, Gillette MA, et al. Gene set enrichment analysis: a knowledge-based approach for interpreting genome-wide expression profiles. Proc Natl Acad Sci U S A 2005;102:15545–50.
12. Lopes CT, Franz M, Kazi F, Donaldson SL, Morris Q, Bader GD. Cytoscape Web: an interactive web-based network browser. Bioinformatics 2010;26:2347–8.
13. Gao H, Korn JM, Ferretti S, Monahan JE, Wang Y, Singh M, et al. High-throughput screening using patient-derived tumor xenografts to predict clinical trial drug response. Nat Med 2015;21:1318–25.
14. Mer AS, Ba-Alawi W, Smirnov P, Wang YX, Brew B, Ortmann J, et al. Integrative pharmacogenomics analysis of patient-derived xenografts. Cancer Res 2019;79:4539–50.
15. Beigbeder A, Velot L, James DA, Bisson N. Sample preparation for mass spectrometry analysis of protein–protein interactions in cancer cell lines and tissues. Methods Mol Biol 2016;1458:339–47.
16. Rappsilber J, Mann M, Ishihama Y. Protocol for micro-purification, enrichment, pre-fractionation, and storage of peptides for proteomics using StageTips. Nat Protoc 2007;2:1896–906.
17. Nesvizhskii AI, Keller A, Kolker E, Aebersold R. A statistical model for identifying proteins by tandem mass spectrometry. Anal Chem 2003;75:4646–58.
18. Teo G, Liu G, Zhang J, Nesvizhskii AI, Gingras AC, Choi H. SAINTexpress: improvements and additional features in significance analysis of INTeractome software. J Proteomics 2014;100:37–43.
19. Perez-Riverol Y, Csordas A, Bai J, Bernal-Llinares M, Hewapathirana S, Kundu DJ, et al. The PRIDE database and related tools and resources in 2019: improving support for quantification data. Nucleic Acids Res 2019;47:D442–D50.
20. Foster LJ, De Hoog CL, Mann M. Unbiased quantitative proteomics of lipid rafts reveals high specificity for signaling factors. Proc Natl Acad Sci U S A 2003;100:5813–8.
21. Ishihama Y, Rappsilber J, Andersen JS, Mann M. Microcolumns with self-assembled particle frits for proteomics. J Chromatogr A 2002;979:233–9.
22. Cox J, Mann M. MaxQuant enables high peptide identification rates, individualized p.p.b.-range mass accuracies and proteome-wide protein quantification. Nat Biotechnol 2008;26:1367–72.
23. Hart T, Brown KR, Sircoulomb F, Rottapel R, Moffat J. Measuring error rates in genomic perturbation screens: gold standards for human functional genomics. Mol Syst Biol 2014;10:733.
24. Cioce M, Fazio VM. EphA2 and EGFR: friends in life, partners in crime. Can EphA2 be a predictive biomarker of response to anti-EGFR agents? Cancers 2021;13:700.
25. Lee H, Bennett AM. Receptor protein tyrosine phosphatase-receptor tyrosine kinase substrate screen identifies EphA2 as a target for LAR in cell migration. Mol Cell Biol 2013;33:1430–41.
26. Yeddula N, Xia Y, Ke E, Beumer J, Verma IM. Screening for tumor suppressors: loss of ephrin receptor A2 cooperates with oncogenic KRas in promoting lung adenocarcinoma. Proc Natl Acad Sci U S A 2015;112:E6476–85.
27. VanderSluis B, Costanzo M, Billmann M, Ward HN, Myers CL, Andrews BJ, et al. Integrating genetic and protein-protein interaction networks maps a functional wiring diagram of a cell. Curr Opin Microbiol 2018;45:170–9.
28. Larsen AB, Stockhausen MT, Poulsen HS. Cell adhesion and EGFR activation regulate EphA2 expression in cancer. Cell Signal 2010;22:636–44.
29. Larsen AB, Pedersen MW, Stockhausen MT, Grandal MV, van Deurs B, Poulsen HS. Activation of the EGFR gene target EphA2 inhibits epidermal growth factor-induced cancer cell motility. Mol Cancer Res 2007;5:283–93.

30. Kim J, Chang IY, You HJ. Interactions between EGFR and EphA2 promote tumorigenesis through the action of Ephexin1. Cell Death Dis 2022;13:528.
31. Amato KR, Wang S, Tan L, Hastings AK, Song W, Lovly CM, et al. EPHA2 blockade overcomes acquired resistance to EGFR kinase inhibitors in lung cancer. Cancer Res 2016;76:305–18.
32. Strimpakos A, Pentheroudakis G, Kotoula V, De Roock W, Kouvatseas G, Papakostas P, et al. The prognostic role of ephrin A2 and endothelial growth factor receptor pathway mediators in patients with advanced colorectal cancer treated with cetuximab. Clin Colorectal Cancer 2013;12:267–74.
33. De Robertis M, Loiacono L, Fusilli C, Poeta ML, Mazza T, Sanchez M, et al. Dysregulation of EGFR pathway in EphA2 cell subpopulation significantly associates with poor prognosis in colorectal cancer. Clin Cancer Res 2017;23: 159–70.
34. Merchant AM, Zhu Z, Yuan JQ, Goddard A, Adams CW, Presta LG, et al. An efficient route to human bispecific IgG. Nat Biotechnol 1998;16:677–81.
35. Banisadr A, Safdari Y, Kianmehr A, Pourafshar M. Production of a germline-humanized cetuximab scFv and evaluation of its activity in recognizing EGFR-overexpressing cancer cells. Hum Vaccin Immunother 2018;14: 856–63.
36. Li R, Huang Y, Lin J. Distinct effects of general anesthetics on lung metastasis mediated by IL6/JAK/STAT3 pathway in mouse models. Nat Commun 2020; 11:642.
37. DeRose YS, Wang G, Lin YC, Bernard PS, Buys SS, Ebbert MT, et al. Tumor grafts derived from women with breast cancer authentically reflect tumor pathology, growth, metastasis, and disease outcomes. Nat Med 2011;17: 1514–20.
38. Wu Q, Qian W, Sun X, Jiang S. Small-molecule inhibitors, immune checkpoint inhibitors, and more: FDA-approved novel therapeutic drugs for solid tumors from 1991 to 2021. J Hematol Oncol 2022;15:143.
39. Fauvel B, Yasri A. Antibodies directed against receptor tyrosine kinases: current and future strategies to fight cancer. MAbs 2014;6:838–51.
40. Quintanal-Villalonga A, Chan JM, Yu HA, Pe'er D, Sawyers CL, Sen T, et al. Lineage plasticity in cancer: a shared pathway of therapeutic resistance. Nat Rev Clin Oncol 2020;17:360–71.
41. Carter PJ, Lazar GA. Next generation antibody drugs: pursuit of the "high-hanging fruit." Nat Rev Drug Discov 2018;17:197–223.
42. Runcie K, Budman DR, John V, Seetharamu N. Bi-specific and tri-specific antibodies—the next big thing in solid tumor therapeutics. Mol Med 2018; 24:50.
43. Suurs FV, Lub-de Hooge MN, de Vries EGE, de Groot DJA. A review of bispecific antibodies and antibody constructs in oncology and clinical challenges. Pharmacol Ther 2019;201:103–19.
44. Moores SL, Chiu ML, Bushey BS, Chevalier K, Luistro L, Dorn K, et al. A novel bispecific antibody targeting EGFR and cMet is effective against EGFR inhibitor-resistant lung tumors. Cancer Res 2016;76:3942–53.
45. Patnaik A, Gordon M, Tsai F, Papadopoulos KP, Rasco D, Beeram M, et al. A phase I study of LY3164530, a bispecific antibody targeting MET and EGFR, in patients with advanced or metastatic cancer. Cancer Chemother Pharmacol 2018;82:407–18.
46. Sellmann C, Doerner A, Knuehl C, Rasche N, Sood V, Krah S, et al. Balancing selectivity and efficacy of bispecific epidermal growth factor receptor (EGFR) x c-MET antibodies and antibody–drug conjugates. J Biol Chem 2016;291: 25106–19.
47. McDaniel NK, Iida M, Nickel KP, Longhurst CA, Fischbach SR, Rodems TS, et al. AXL mediates cetuximab and radiation resistance through tyrosine 821 and the c-ABL kinase pathway in head and neck cancer. Clin Cancer Res 2020;26: 4349–59.
48. Rau A, Lieb WS, Seifert O, Honer J, Birnstock D, Richter F, et al. Inhibition of tumor cell growth and cancer stem cell expansion by a bispecific antibody targeting EGFR and HER3. Mol Cancer Ther 2020;19:1474–85.
49. Yun J, Lee SH, Kim SY, Jeong SY, Kim JH, Pyo KH, et al. Antitumor activity of amivantamab (JNJ-61186372), an EGFR-cMet bispecific antibody, in diverse models of EGFR exon 20 insertion-driven NSCLC. Cancer Discov 2020;10:1194–1209.
50. Pottier C, Fresnais M, Gilon M, Jerusalem G, Longuespee R, Sounni NE. Tyrosine kinase inhibitors in cancer: breakthrough and challenges of targeted therapy. Cancers 2020;12:731.
51. Parseghian CM, Napolitano S, Loree JM, Kopetz S. Mechanisms of innate and acquired resistance to anti-EGFR therapy: a review of current knowledge with a focus on rechallenge therapies. Clin Cancer Res 2019;25:6899–908.
52. Liu Q, Yu S, Zhao W, Qin S, Chu Q, Wu K. EGFR-TKIs resistance via EGFR-independent signaling pathways. Mol Cancer 2018;17:53.